

Tilt Measurement at the Quantum Cramer–Rao Bound Using a Higher-Order Hermite–Gaussian Mode

Zhi Li ^{1,2}, Yijian Wang ^{1,2}, Hengxin Sun ^{1,2,*}, Kui Liu ^{1,2}  and Jiangrui Gao ^{1,2}

¹ State Key Laboratory of Quantum Optics and Quantum Optics Devices, Institute of Opto-Electronics, Shanxi University, Taiyuan 030006, China

² Collaborative Innovation Center of Extreme Optics, Shanxi University, Taiyuan 030006, China

* Correspondence: hxsun@sxu.edu.cn

Abstract: The quantum Cramer–Rao bound (QCRB) provides an ultimate precision limit in parameter estimation. The sensitivity of spatial measurements can be improved by using the higher-order Hermite–Gaussian mode. However, to date, the QCRB-saturating tilt measurement has not been realized. Here, we experimentally demonstrate tilt measurements using a higher-order HG_{40} mode as the probe beam. Using the balanced homodyne detection with an optimal local beam, which involves the superposition of high-order HG_{30} and HG_{50} modes, we demonstrate the precision of the tilt measurement approaching the QCRB. The signal-to-noise ratio of the tilt measurement is enhanced by 9.2 dB compared with the traditional method using HG_{00} as the probe beam. This scheme is more practical and robust to losses, which has potential applications in areas such as laser interferometer gravitational-wave observatories and high-sensitivity atomic force microscopes.

Keywords: high-order Hermite–Gaussian mode; tilt measurement; quantum Cramer–Rao bound; homodyne detection

1. Introduction

The high-precision measurement of transverse displacement and tilt of an optical beam has applications in several areas, such as the laser interferometer gravitational-wave observatory (LIGO) detector [1], biological measurements [2,3], satellite positioning [4,5], and atomic force microscopy [6]. Different from the longitudinal optical phase measurement, this generally involves the transverse complex amplitude distribution of a laser beam, spatial detection methods, such as quadrant detectors, or spatial mode-based homodyne detection using high-order modes. Mode matching is crucial in such ultrasensitive spatial detections. Therefore, the optimal detection scheme with ideal mode matching is required to reach the ultimate measurable quantum limit.

Several methods are proposed to enhance the spatial measurements [7,8]. One involves using non-classical light, such as spatial squeezing, to decrease the quantum noise below the shot noise limit [9,10]. For example, by coupling a squeezed high-order mode squeezing into a fundamental mode laser beam, a spatially squeezed beam can be used as the probe to perform a transverse displacement beyond the standard quantum limit [11–13]. This quantum technique was also demonstrated in the biological measurement beyond the quantum limit [3] and in the spatial entanglement characterization [14]. Recently, there have been experimental demonstrations of higher-order spatially squeezed beams, showing that a higher-order spatially squeezed beam is an effective probe beam used to boost the precision of spatial tilt and displacement measurements [15].

Another method involves increasing the spatial detection efficiency. A split detection scheme with a quadrant photodetector is often used in transverse displacement detection. However, split detection is proved to be only 64% efficient compared to the newly proposed scheme of the so-called TEM_{10} homodyne detection, where a TEM_{10} mode local oscillator



Citation: Li, Z.; Wang, Y.; Sun, H.; Liu, K.; Gao, J. The Tilt Measurement at the Quantum Cramer–Rao Bound Using a Higher-Order Hermite–Gaussian Mode. *Photonics* **2023**, *10*, 584. <https://doi.org/10.3390/photonics10050584>

Received: 10 April 2023

Revised: 14 May 2023

Accepted: 15 May 2023

Published: 17 May 2023



Copyright: © 2023 by the authors. Licensee MDPI, Basel, Switzerland. This article is an open access article distributed under the terms and conditions of the Creative Commons Attribution (CC BY) license (<https://creativecommons.org/licenses/by/4.0/>).

interferes with the fundamental mode probe to obtain the displacement information [16,17]. Recently, parallel research on weak value-based measurements also improved the signal-to-noise ratio (SNR) of optical tilt measurements with a TEM_{10} homodyne detection [18].

One more method involves using the high-order mode as the probe beam. The higher-order mode contains more Fisher information for a spatial measurement [19,20] and, thus, has an improved spatial sensitivity compared with a lower-order one. This scheme was proposed and experimentally demonstrated using the HG_{10} mode as the probe and HG_{20} mode as the local oscillator. Although an improvement factor of 1.41 was demonstrated, the HG_{20} mode is actually not the optimal local mode used to obtain the transverse information of the HG_{10} mode [21]. The quantum spatial scheme was also demonstrated with high-order modes, while the optimal local modes were not used [18]. The optimal local modes with high-order modes can increase the spatial detection efficiency, similar to the role that the TEM_{10} homodyne detection plays instead of the split detection. The sensitivity of the high-order mode-based scheme is ultimately determined by the quantum Cramer–Rao bound (QCRB), which is closely related to the local mode selection of homodyne detection.

In this paper, we experimentally demonstrated the tilt measurement with a higher-order $HG_{m,0}$ ($m = 0, 1, 2, 3, 4$) mode as the probe beam. Using the balanced homodyne detection with an optimal local mode, which is the superposition of the high-order $HG_{m+1,0}$ and $HG_{m-1,0}$ modes, we demonstrated the precision of the tilt measurement approaching the QCRB. With $m = 4$, the SNR of the tilt measurement is enhanced by 9.2 dB compared to the traditional method using HG_{00} as the probe beam.

2. Theoretical Model

The tilt of a high-order Hermite–Gauss (HG) mode is shown in Figure 1. Here, the tilt is defined with respect to a pivot point centered on the beam waist. The transverse complex amplitude distribution of a tilted beam with an arbitrary mode order can be regarded as adding an extra propagating phase, and is given by

$$u_p(x) = e^{i\frac{2\pi \sin \theta}{\lambda}x}u(x \cos \theta), \tag{1}$$

where $u(x)$ is the transverse complex amplitude distribution of the original HG mode, λ is the optical wavelength, and p is the transverse momentum of the beam. In the case of the small tilt angle, we have $p = 2\pi \sin \theta / \lambda \approx 2\pi\theta / \lambda$.

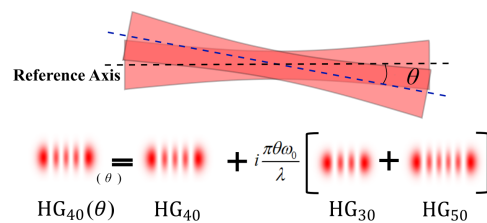


Figure 1. The tilt of the high-order Hermite–Gaussian beam. A tilted HG_{40} mode beam is decomposed in the HG_{40} , HG_{30} , and HG_{50} mode components. The tilt information θ is carried by the combination of HG_{30} and HG_{50} modes. The ω_0 is the beam waist of the incident HG_{00} mode.

Then Equation (1) becomes

$$u_p(x) \approx u(x) + i\frac{2\pi\theta}{\lambda}x \cdot u(x). \tag{2}$$

The transverse complex amplitude distribution of an n th-order HG beam can be written as

$$u_n(x) = \left(\frac{2}{\pi\omega_0^2}\right)^{\frac{1}{4}} \frac{1}{\sqrt{n!2^n}} H_n\left(\frac{\sqrt{2}x}{\omega_0}\right) e^{-\left(\frac{x}{\omega_0}\right)^2}, \tag{3}$$

where ω_0 is the beam waist related to the corresponding fundamental mode, and $H_n(X)$ is the Hermitian polynomial, where n represents the mode order.

Substituting Equation (3) into Equation (2), we have

$$u_n(x, p) \approx u_n(x) + i\frac{2\pi\theta}{\lambda}xu_n(x) = u_n(x) + i\frac{\pi\theta\omega_0}{\lambda}(\sqrt{n+1}u_{n+1}(x) + \sqrt{n}u_{n-1}(x)), \quad (4)$$

where $xu_n(x) = \omega_0(\sqrt{n+1}u_{n+1}(x) + \sqrt{n}u_{n-1}(x))/2$ with $n \geq 1$. We can see that the tilt information θ is carried by the $HG_{n+1,0}$ and $HG_{n-1,0}$ modes, which are called the detection modes in some literature [22].

In the quantum regime, the positive frequency part of an electric field operator of the probe beam can be written as [17]

$$\hat{\varepsilon}^+(x) = i\sqrt{\frac{\hbar\omega}{2\varepsilon_0cT}} \sum_{n=0}^{\infty} \hat{a}_n u_n(x), \quad (5)$$

where \hbar is the reduced Planck constant, ω is the frequency of the light field, ε_0 is the vacuum permittivity, c is the speed of light, and T is the detection time. \hat{a}_n is the annihilation operator corresponding to the n th order mode, $\hat{a}_n = (\hat{X}_n^+ + i\hat{X}_n^-)/2$ could be written as a linearized form of $\hat{a}_n = \langle \hat{a}_n \rangle + \delta\hat{a}_n$, where $\langle \hat{a}_n \rangle$ is the classical amplitude and $\delta\hat{a}_n$ is the quantum noise operator.

When the probe beam is a bright $HG_{n,0}$ mode, $\langle \hat{a}_n \rangle = \sqrt{N}$, N is the photon number of the $HG_{n,0}$ mode. All of the other modes are in the vacuum state. Equation (5) can be rewritten as

$$\hat{\varepsilon}^+(x) = i\sqrt{\frac{\hbar\omega}{2\varepsilon_0cT}} \left\{ \sqrt{N}u_n(x) + \sum_{m=0}^{\infty} \delta\hat{a}_m u_m(x) \right\}. \quad (6)$$

The probe beam undergoes a small tilt angle, say θ , we have

$$\hat{\varepsilon}_\theta^+(x) = i\sqrt{\frac{\hbar\omega}{2\varepsilon_0cT}} \left\{ \sqrt{N}[u_n(x) + i\frac{\pi\theta\omega_0}{\lambda}(\sqrt{n+1}u_{n+1}(x) + \sqrt{n}u_{n-1}(x))] + \sum_{m=0}^{\infty} \delta\hat{a}_m u_m(x) \right\}. \quad (7)$$

It is proved that a balanced homodyne detection (BHD) with the “detection mode” as the local oscillator can reach the QCRB of a spatial measurement [22]. The normalized mode of the local oscillator is the superposition of the high-order $HG_{n+1,0}$ and $HG_{n-1,0}$ modes, written as

$$u^{LO}(x) = \frac{[\sqrt{n+1} \cdot u_{n+1}(x) + \sqrt{n} \cdot u_{n-1}(x)]}{\sqrt{2n+1}}. \quad (8)$$

The local oscillator field is then written as

$$\hat{\varepsilon}_{Local}^+(x) = i\sqrt{\frac{\hbar\omega}{2\varepsilon_0cT}} \left[\sqrt{N_{LO}}u_{LO}(x) + \sum_{m=0}^{\infty} \delta\hat{a}_m^{LO} u_m(x) \right], \quad (9)$$

where N_{LO} is the mean photon number of the local oscillator.

According to the beam splitter model, the light field operators on the two detectors of BHD can be written as

$$\hat{\varepsilon}_A^+(x) = (\hat{\varepsilon}_\theta^+(x) + \hat{\varepsilon}_{LO}^+(x))/\sqrt{2}, \quad (10)$$

$$\hat{\varepsilon}_B^+(x) = (\hat{\varepsilon}_\theta^+(x) - \hat{\varepsilon}_{LO}^+(x))/\sqrt{2}. \quad (11)$$

The output photon number of the BHD system is given by

$$\hat{n}_- = \frac{2\varepsilon_0 c T}{\hbar \omega} \left[\int_{-\infty}^{+\infty} (\hat{\varepsilon}_A^+(x))^\dagger (\hat{\varepsilon}_A^+(x)) dx - \int_{-\infty}^{+\infty} (\hat{\varepsilon}_B^+(x))^\dagger (\hat{\varepsilon}_B^+(x)) dx \right]. \tag{12}$$

Substituting Equations (7) and (9) into Equation (12), we have

$$\hat{n}_- = \sqrt{N_{LO}} \left(\frac{2\pi\theta\omega_0\sqrt{N}\sqrt{2n+1}}{\lambda} + \delta\hat{X}_s^- \right), \tag{13}$$

where $\delta\hat{X}_s^-$ is the quantum noise of the signal beam and is related to the “detection mode”. In Equation (13), the first term represents the signal, and the second term represents noise. For coherent light ($\langle \delta^2\hat{X}_s^- \rangle = 1$), the signal-to-noise ratio (SNR) is defined as

$$SNR^{opt} = \left(\frac{2\pi\theta\omega_0\sqrt{N}\sqrt{2n+1}}{\lambda} \right)^2. \tag{14}$$

When we choose an intermediate mode $HG_{n+1,0}$ as the local oscillator, i.e., $u_{int}^{LO}(x) = u_{n+1}(x)$, the corresponding BHD output and SNR are, respectively, given by

$$\hat{n}_- = \sqrt{N_{LO}} \left(\frac{2\pi\theta\omega_0\sqrt{N}\sqrt{n+1}}{\lambda} + \delta\hat{X}_s^- \right), \tag{15}$$

$$SNR^{int} = \left(\frac{2\pi\theta\omega_0\sqrt{N}\sqrt{n+1}}{\lambda} \right)^2. \tag{16}$$

We plot the SNRs varying with the mode order using the logarithmic scale in Figure 2, with circle dots and square dots, respectively, corresponding to Equations (14) and (16). Both are normalized to $(2\pi\theta\sqrt{N}\omega_0/\lambda)^2$, which represents the SNR with the coherent HG_{00} signal mode. Both SNRs increase with the mode order increasing. The SNR of the optimal scheme indicates an improvement of $(2n + 1)$ for the n th-order mode compared to the fundamental mode. Furthermore, the SNR of the optimal scheme is higher than that of the intermediate one for any high-order mode. For example, with the first-order mode probe, the SNR of optimal BHD is 1.5 times that of the SNR of the intermediate BHD.

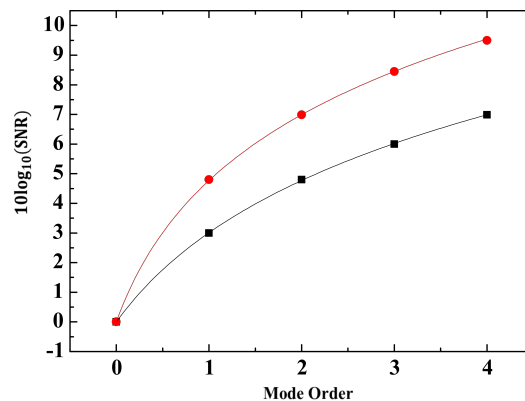


Figure 2. Mode–order dependence of the normalized SNRs for the optimal (red circle dots) and intermediate (black square dots) balanced homodyne detection.

We derive the QCRB of the tilt measurement by using a similar method to Reference [22]. We use the minimum measurable tilt to characterize the measurement precision. For the

optimal BHD measurement discussed above, the minimum measurable tilt is defined as the tilt with $SNR = 1$. According to Equation (14), the minimum measurable tilt is given by

$$\theta_{min}^{opt} = \frac{\lambda}{2\pi\omega_0\sqrt{2n+1}\sqrt{N}}. \tag{17}$$

The precision of the estimation of any physical parameter φ is limited by the Cramer–Rao bound and only depends on properties of the probe beam, such as the intensity, beam profile, and the quantum fluctuations. Furthermore, the variance of any unbiased estimator of φ is necessarily greater than $1/I_F$, where I_F is the Fisher information [23]. The minimum measurable information of any parameter φ is bounded by the quantum Cramer–Rao bound [22]

$$\delta\varphi \geq \delta\varphi_{min} = \frac{\sigma_{min}}{\sqrt{QN_\varphi}} \left[4\|u'_{\varphi=0}\|^2 + \frac{N'_{\varphi}}{N_\varphi} \right]^{-1/2}, \tag{18}$$

where $\delta\varphi_{min}$ is the best achievable sensitivity for measuring a small variation of φ , σ_{min} is the quantum noise, N_φ is the mean photon number, N'_{φ} is its derivative with respect to φ , Q is the number of measurement repetitions, and $u'_{\varphi=0}$ is the derivative of the normalized transverse field distribution u_φ with respect to φ at $\varphi = 0$.

For tilt measurements with the high-order $HG_{n,0}$ probe beam, φ is replaced by the tilt θ , $\|u'_{\theta}\|^2 = \|\partial[u_n(x,p)]/\partial\theta|_{\theta=0}\|^2 = \pi^2\omega_0^2(2n+1)/\lambda^2$, $N'_\theta = 0$, $\sigma_{min} = 1$ as the coherent light is used. We then obtain the QCRB for the tilt measurement of

$$\theta_{min}^{QCR} = \frac{\lambda}{2\pi\omega_0\sqrt{2n+1}\sqrt{N}}. \tag{19}$$

By comparing Equations (17) and (19), we can see that the optimal BHD scheme reaches the QCRB.

In fact, for the probe beam of the fundamental mode, the $HG_{1,0}$ mode itself is the optimal local oscillator, as there is no lower mode than zero. That is why, in References [16,17], the sensitivity of displacement and tilt measurements at the Cramer–Rao Bound can be achieved for $HG_{0,0}$ probe beams using only $HG_{1,0}$ mode homodyne detection. However, for higher-order modes other than the fundamental mode, only the superposition mode (formed by the combination of two modes as the local oscillator) can reach the QCRB. We experimentally verify this theory by utilizing a probe beam that consists of modes up to the fourth order in the following.

3. Experimental Setup and Results

We use different high-order HG modes as probe beams for tilt measurements, and apply spatially balanced homodyne detection (BHD) with intermediate and optimal local modes, respectively. The experimental setup is illustrated in Figure 3. A laser beam from an 1080 nm optical fiber laser is split into three beams, one is mode-converted into the $HG_{n,0}$ mode as the probe by a mode converter (MC_3). The other two beams are, respectively, mode-converted into the $HG_{n+1,0}$ mode and $HG_{n-1,0}$ mode by two mode converters ($MC_{1,2}$). Then the two modes of $HG_{n+1,0}$ and $HG_{n-1,0}$ are coupled on a BS_3 to produce the optimal local oscillator.

The probe beam passes through a tilt modulator, which is made of a wedged electro-optic crystal to perform a pure tilt modulation [24]. The tilted $HG_{n,0}$ mode and optimal local beam are coupled on a 50/50 beam splitter (BS_4) for optimal BHD to demodulate the tilt signals. In the intermediate BHD, the $HG_{n-1,0}$ mode is blocked; only the $HG_{n+1,0}$ mode is left to be the local oscillator to demodulate the tilt signals.

The wedged crystal is driven by a sine wave signal to simulate a slight tilt signal at 3 MHz. The experimental parameters are as follows: the signal beam power, $P_s = 30 \mu\text{W}$; the modulation peak-to-peak voltage is 3 V; the beam waist of $HG_{0,0}$, $\omega_0 = 220 \mu\text{m}$; the resolution bandwidth of the spectrum analyzer, $\text{RBW} = 30 \text{ kHz}$; the video bandwidth,

VBW = 300 Hz; and the analyzing frequency, $f = 3$ MHz. In Figure 3, we select the probe beam with a mode order of $n = 4$.

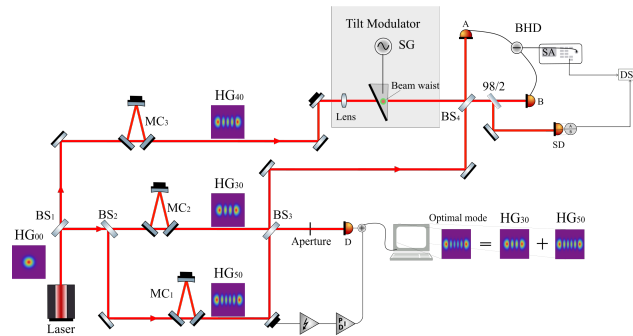


Figure 3. Experimental setup for tilt measurements with different high-order HG modes. Mode converter (MC), detector(D), beam splitter (BS), signal generator (SG), balanced homodyne detection (BHD), 50/50 beam splitter (BS), digital storage oscilloscope (DSO), and split detector (SD).

As shown in Figure 3, the small fraction of the optimal local beam passed through an aperture to extract the interference signal, which is used for the feedback control of the relative phase between the $HG_{n+1,0}$ and $HG_{n-1,0}$ modes. The relative phase between the $HG_{n+1,0}$ and $HG_{n-1,0}$ modes was locked to $\phi = 0$ and the power ratio of $HG_{n+1,0}$ and $HG_{n-1,0}$ modes is $(n + 1)/(n - 1)$. A small part (2%) separated from one beam of BHD is used to construct the 4F phase monitoring system to check the tilt signal of a laser probe beam [24]. The demodulated tilt signal from the spectrum analyzer (trace1) and the interference signal (trace2) from the 4F monitoring system are shown in Figure 4, with the scanning local phase. The tilt signal appears, approximately, at the interfering phase of $\phi = \pi/2$, which is consistent with the theory.

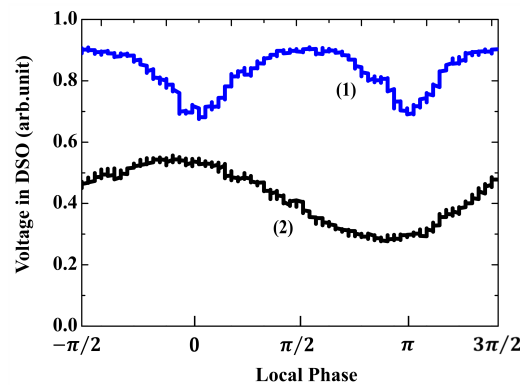


Figure 4. The phase monitoring from the digital storage oscilloscope (DSO) for the demodulated tilt signal. Trace1 represents the demodulated signals by the spectrum analyzer (SA). Trace2 represents the interference signals from one half of the split detector.

The experimental results of the demodulated tilt signal from the spectrum analyzer are shown in Figure 5. With probe beams of the same optical power but different modes, the shot noise limits (SNLs) are the same, shown by trace1 in any single measurement, and obtained by switching off the tilt modulation. Trace2 corresponds to the tilt signals with the scanning phase of the local beam. The tilt modulation depths are the same for all of the measurements. With the traditional scheme with the $HG_{0,0}$ mode as the probe and the $HG_{1,0}$ mode as the local oscillator, the total power of the tilt signal of 6.6 dB above the SNL is shown in Figure 5a. The results for the $HG_{1,0}$, $HG_{2,0}$, $HG_{3,0}$, and $HG_{4,0}$ modes as the probes, with an intermediate high-order mode as the local oscillator, are shown in Figure 5b–e. The total powers of the tilt signal are, respectively, 8.9 dB, 10.5 dB, 11.8 dB, and 12.6 dB above the SNL. The results of the $HG_{1,0}$ to $HG_{4,0}$ modes as the probes, and the

superpositions of high-order modes as local oscillators, are shown in Figure 5f–i. The total powers of the tilt signal are, respectively, 10.6 dB, 12.7 dB, 14.1 dB, and 14.8 dB above the SNL. The results of the intermediate and optimal BHD are, respectively, shown in the red and green boxes.

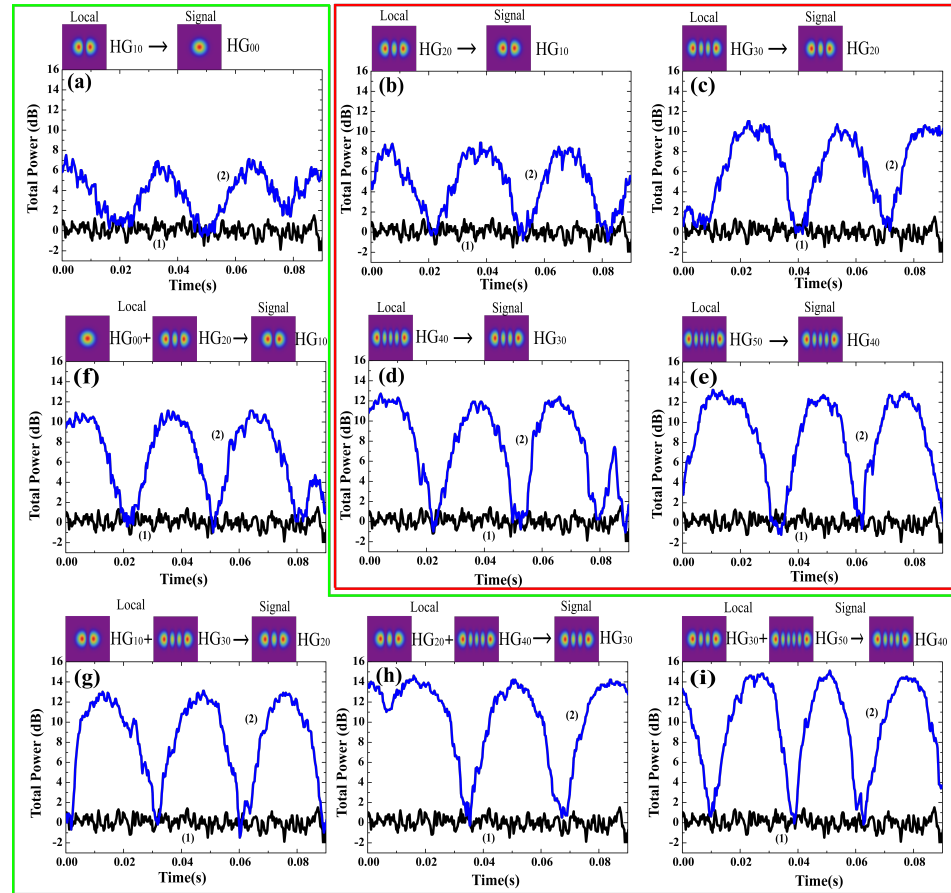


Figure 5. The different high-order HG modes as the probe beam vs. the total power of the tilt signal. (a) The $HG_{0,0}$ mode as the probe and the $HG_{1,0}$ mode as the local oscillator. (b–e) The $HG_{1,0}$ to $HG_{4,0}$ modes as the probes, with the intermediate high-order modes as the local oscillators. (f–i) The $HG_{1,0}$ to $HG_{4,0}$ modes as the probes, and the optimal high-order modes as local oscillators. Trace1 (black line) is the shot noise level with the signal beam being blocked. Trace2 (blue line) corresponds to the total power of the tilt signal with the scanning of the phase of the local beam.

The SNRs derived from the total powers, which vary with the mode orders of the probes, are shown in Figure 6, along with the optimal BHD (blue circle dots) and intermediate BHD (black square dots), respectively. The corresponding fitting results are shown in red lines. With the increasing mode order of the probe and with the optimal BHD, the SNRs become higher, showing a good agreement with the theoretical prediction. Furthermore, the results of the optimal BHD reach the quantum Cramer–Rao bound. For example, with the $HG_{4,0}$ mode as the probe beam, the SNR of the optimal BHD is 9.2 dB above the shot noise limit (SNL), which approaches the ultimate value of 9.5 dB. The results show an improvement of 2.3 dB compared to the intermediate BHD scheme, indicating great potential for future applications.

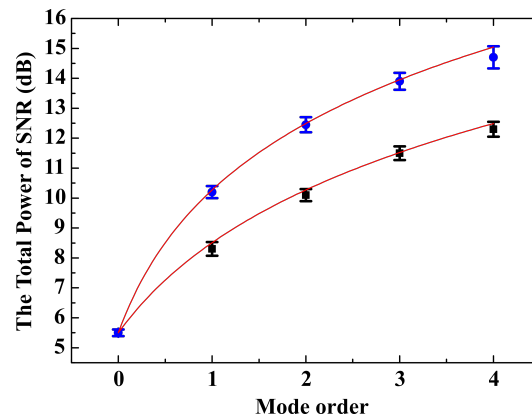


Figure 6. The total power of SNR with different probe beams. The circle dots and square dots, respectively, represent the experimental results with an optimal BHD and intermediate BHD. The red lines are the theoretical fittings.

4. Conclusions

We have theoretically analyzed optical tilt measurements using higher-order Hermite–Gauss modes. Using a probe beam that includes modes up to the fourth order, we experimentally demonstrated the tilt measurement by the optimal BHD. The results show that the tilt measurement precision reaches the so-called quantum Cramer–Rao bound. Compared to the traditional scheme of the $HG_{0,0}$ mode, with the $HG_{4,0}$ mode as the probe beam, the SNR is enhanced by 9.2 dB, which is in good agreement with the theory (9.5 dB). The enhancement is equivalent to using a 9.2 dB spatially squeezed light as the probe beam, but is more practical and robust to losses. This high-order mode-based scheme has potential applications in areas such as laser interferometer gravitational-wave observatories and high-sensitivity atomic force microscopes [6,25].

Author Contributions: Conceptualization, H.S., K.L. and J.G.; methodology, Z.L. and H.S.; software, Z.L. and Y.W.; validation, Z.L.; formal analysis, Z.L. and H.S.; investigation, Z.L. and H.S.; data curation, Z.L. and H.S.; writing—original draft preparation, Z.L.; writing—review and editing, Z.L. and H.S.; funding acquisition, H.S., K.L. and J.G. All authors have read and agreed to the published version of the manuscript.

Funding: This research was supported by the Shanxi Scholarship Council of China (2021-05); the National Natural Science Foundation of China (91536222, 12074233); and the National Key Research and Development Program of China (2021YFC2201802).

Institutional Review Board Statement: Not applicable.

Informed Consent Statement: Not applicable.

Data Availability Statement: The data that support the findings of this study are available from the corresponding authors upon reasonable request.

Conflicts of Interest: The authors declare no conflict of interest.

References

1. Coddington, I.; Swann, W.; Nenadovic, L.; Newbury, N. Rapid and precise absolute distance measurements at long range. *Nat. Photonics* **2008**, *10*, 142–149. [[CrossRef](#)]
2. Tischer, C.; Altmann, S.; Hoerber, J.; Stelzer, E.; Florin, E. Three-dimensional thermal noise imaging. *Appl. Phys. Lett.* **2001**, *79*, 3878. [[CrossRef](#)]
3. Taylor, M.; Janousek, J.; Daria, V.; Knittel, J.; Hage, B.; Bachor, H.; Bowen, W. Biological measurement beyond the quantum limit. *Nat. Photonics* **2013**, *7*, 299. [[CrossRef](#)]
4. Arnon, S. Use of satellite natural vibrations to improve performance of free-space satellite laser communication. *Appl. Opt.* **1998**, *37*, 5031–5036. [[CrossRef](#)] [[PubMed](#)]
5. Nikulin, V.; Bouzoubaa, M.; Skormin, V.; Busch, T. Modeling of the tracking system components of the laser satellite communication systems. *Opt. Eng.* **2001**, *40*, 72–82. [[CrossRef](#)]

6. Putman, C.; Grooth, B.; Van, H.; Greve, J. A detailed analysis of the optical beam deflection technique for use in atomic force microscopy. *J. Appl. Phys.* **1992**, *72*, 6. [[CrossRef](#)]
7. Fabre, C.; Fouet, J.; Maitre, A. Quantum limits in the measurement of very small displacements in optical images. *Opt. Lett.* **2000**, *25*, 76–78. [[CrossRef](#)]
8. Treps, N.; Grosse, N.; Bowen, W.; Hsu, M.; Maitre, A.; Fabre, C.; Bachor, H.; Lam, P. Nano-displacement measurements using spatially multimode squeezed light. *J. Opt. B Quantum Semiclass. Opt.* **2004**, *6*, S664. [[CrossRef](#)]
9. Gao, Y.; Kuang, L. Optimal quantum estimation of the displacement in optical imaging. *J. Phys. B At. Mol. Opt. Phys.* **2019**, *52*, 215403. [[CrossRef](#)]
10. Pooser, R.; Savino, N.; Batson, E.; Beckey, J.; Garcia, J.; Lawrie, B. Truncated nonlinear interferometry for quantum-enhanced atomic force microscopy. *Phys. Rev. Lett.* **2020**, *124*, 230504. [[CrossRef](#)]
11. Treps, N.; Andersen, U.; Buchler, B.; Lam, P.; Maitre, A.; Bachor, H.; Fabre, C. Surpassing the standard quantum limit for optical imaging using nonclassical multimode light. *Phys. Rev. Lett.* **2002**, *88*, 203601. [[CrossRef](#)]
12. Treps, N.; Grosse, N.; Bowen, W.; Fabre, C.; Bachor, H.; Lam, P. A Quantum Laser Pointer. *Science* **2008**, *301*, 940. [[CrossRef](#)] [[PubMed](#)]
13. Sun, H.; Liu, Z.; Liu, K.; Yang, R.; Zhang, J.; Gao, J. Experimental Demonstration of a Displacement Measurement of an Optical Beam beyond the Quantum Noise Limit. *Chin. Phys. Lett.* **2014**, *31*, 084202. [[CrossRef](#)]
14. Wagner, K.; Janousek, J.; Delaubert, V.; Zou, H.; Harb, C.; Treps, N.; Morizur, J.; Lam, P.; Bachor, H. Entangling the spatial properties of laser beams. *Science* **2008**, *321*, 541–543. [[CrossRef](#)] [[PubMed](#)]
15. Li, Z.; Guo, H.; Liu, H.; Li, J.; Sun, H.; Yang, R.; Liu, K.; Gao, J. Higher-Order Spatially Squeezed Beam for Enhanced Spatial Measurements. *Adv. Quantum Technol.* **2022**, *5*, 2200055. [[CrossRef](#)]
16. Hsu, M.; Delaubert, V.; Lam, P.; Bowen, W. Optimal optical measurement of small displacements. *J. Opt. B Quantum Semiclass. Opt.* **2004**, *6*, 495–501. [[CrossRef](#)]
17. Delaubert, V.; Treps, N.; Lassen, M.; Harb, C.; Fabre, C.; Lam, P.; Bachor, H. TEM_{10} homodyne detection as an optimal small-displacement and tilt-measurement scheme. *Phys. Rev. A* **2006**, *75*, 053823. [[CrossRef](#)]
18. Zhang, C.; Lai, Y.; Yang, R.; Liu, K.; Zhang, J.; Sun, H.; Gao, J. Small-tilt measurement based on weak-value-amplification with balanced homodyne detection. *Appl. Phys. Lett.* **2023**, *122*, 031107. [[CrossRef](#)]
19. Xia, B.; Huang, J.; Li, H.; Liu, M.; Xiao, T.; Fang, C.; Zeng, G. Ultrasensitive Measurement of Angular Rotations via Hermite-Gaussian Pointer. *Photonics Res.* **2022**, *10*, 2816. [[CrossRef](#)]
20. Yang, F.; Taschilina, A.; Moiseev, E.; Simon, C.; Lvovsky, A. Far-field linear optical superresolution via heterodyne detection in a higher-order local oscillator mode. *Optica* **2016**, *3*, 1148–1152. [[CrossRef](#)]
21. Sun, H.; Liu, K.; Liu, Z.; Guo, P.; Zhang, J.; Gao, J. Small-displacement measurements using high-order Hermite-Gauss modes. *Appl. Phys. Lett.* **2014**, *104*, 121908. [[CrossRef](#)]
22. Pinel, O.; Fade, J.; Braun, D.; Jian, P.; Treps, N.; Fabre, C. Ultimate sensitivity of precision measurements with intense Gaussian quantum light: A multimodal approach. *Phys. Rev. A* **2012**, *85*, 010101. [[CrossRef](#)]
23. Delaubert, V.; Treps, N.; Fabre, C.; Bachor, H.; Réfrégier, P. Quantum limits in image processing. *Europhys. Lett.* **2008**, *81*, 44001. [[CrossRef](#)]
24. Sun, H.; Li, Z.; Guo, H.; Liu, K.; Gao, J. Pure Modulation and Accurate Measurement of Optical Beam's Tilt and Displacement. *Rev. Sci. Instrum.* **2021**, *92*, 064504. [[CrossRef](#)] [[PubMed](#)]
25. Pooser, R.; Lawrie, B. Ultrasensitive measurement of MEMS cantilever displacement sensitivity below the shot noise limit. *Optica* **2015**, *2*, 393. [[CrossRef](#)]

Disclaimer/Publisher's Note: The statements, opinions and data contained in all publications are solely those of the individual author(s) and contributor(s) and not of MDPI and/or the editor(s). MDPI and/or the editor(s) disclaim responsibility for any injury to people or property resulting from any ideas, methods, instructions or products referred to in the content.